31p

NASA TECHNICAL MEMORANDUM

(NASA TM X-52017)

NASA TM X-52017

GRADUAL TRANSITION OF NUCLEATE BOILING FROM DISCRETE-BUBBLE REGIME TO MULTIBUBBLE REGIME

1609742

by Yih-Yun Hsu
NASA Lewis Research Center
Cleveland, Ohio

1964 31p refs

Presented at [redacted]

TECHNICAL PREPRINT prepared for Heat Transfer Conference and Products Show sponsored by the American Institute of Chemical Engineers and the American Society of Mechanical Engineers
Cleveland, Ohio, August 9-12, 1964

Preprint

NATIONAL AERONAUTICS AND SPACE ADMINISTRATION · WASHINGTON, D.C. · 1964

TECHNICAL MEMORANDUM

GRADUAL TRANSITION OF NUCLEATE BOILING FROM DISCRETE-BUBBLE REGIME TO MULTIBUBBLE REGIME

by Yih-Yun Hsu
Lewis Research Center
Cleveland, Ohio

TECHNICAL PREPRINT prepared for

Heat Transfer Conference and Products Show
sponsored by the American Institute of Chemical Engineers
and the American Society of Mechanical Engineers
Cleveland, Ohio, August 9-12, 1964

NATIONAL AERONAUTICS AND SPACE ADMINISTRATION

GRADUAL TRANSITION OF NUCLEATE BOILING FROM DISCRETE-BUBBLE REGIME TO MULTIBUBBLE REGIME

by Yih-Yun Hsu

Lewis Research Center

ABSTRACT

A photographic study was made of over 5000 bubbles in the nucleate boiling of methanol and water on a narrow heating strip at various heat fluxes and degrees of subcooling. The result showed that transition from the discrete-bubble regime to the multibubble regime was gradual. The fraction of heating area covered by multibubbles increases with the increasing heat flux and is predictable. The area fraction is a Poisson function of the product of the mean area of influence of single bubbles and the instantaneous population density.

ACKNOWLEDGEMENT

The author wishes to thank Mr. R. R. Sharp for his assistance in carrying out the experiment and to the staff of Computing Section B, especially to Miss Eileen Norris, for performing the painstaking and tedious task of analyzing all the bubbles.

INTRODUCTION

Since the nucleate boiling is recognized as a very effective means of heat transfer, a tremendous amount of effort has been directed toward the understanding of this interesting phenomenon. Among such efforts, a good part has been devoted to the study of bubbles. To facilitate observation, studies usually were made on discrete bubbles. Thus, the

formulation of theories on nucleate boiling were based upon the information derived from discrete bubbles (refs. 1 to 3). These theories were generally applied to the entire regime of nucleate boiling. However, recently it has been becoming more and more clear that there actually exist several subdivisions in nuclear boiling; namely, a discrete bubble regime, a merging bubble regime, and perhaps a vapor-patch regime (refs. 4 to 7). It is evident that theories should be developed to deal with each region individually, as well as to predict the transition from one region to another.

It is the purpose of this paper to study the transition of the discrete-bubble regime to the merging-bubble regime. In reference 8, an abrupt transition point was proposed, while in reality the transition is gradual and continuous. This paper will show how the area covered by merging bubbles gradually increases with increasing heat flux, and that the area fractions for merging bubbles can be related with other parameters such as bubble size and instantaneous bubble population. The hope is that if the area fractions covered by the merging bubbles and the discrete-bubbles at a given condition are known, the overall heat-transfer coefficient can be synthesized by weighting the contributions due to the two bubbling mechanisms according to their respective area fractions.

The experimental phase of this work consisted of a photographic study of nucleate boiling of methanol and water on a $\frac{1}{16}$- by $\frac{3}{4}$-inch heating strip under 1 atmosphere pressure. The resulting data were then analyzed by assuming a Poisson distribution of bubbles.

NOMENCLATURE

A	area
a	empirical area parameter used in equation (1)
a,b	empirical parameters used for bubble growth rate $R = at^b$
D	bubble diameter
f	bubble generating frequency
g	gravitational acceleration
h	total number of all single bubbles studied in one roll of film
K	thermal conductivity
k	number of sample frames
L	length of heating strip
M	average number of sites per cell
N	site population
n	instantaneous bubble population
P	probability according to Poisson function
q	heat flux
R	bubble radius
$\dot{R}$	bubble growth rate, dR/dt
s	standard deviation associated with average area fraction of merging bubbles
ΔT_{sub}	subcooling temperature difference between saturation and bulk temperatures
ΔT_w	temperature difference between surface and bulk
t	time
t_g	bubble growth period

t_w waiting period

W half-width of heating strip

X number of bubble sites per cell

x number of bubbles in a cell

β contact angle, radians

δ thermal layer thickness

λ latent heat of vaporization

μ average number of bubbles per cell

ρ density

σ surface tension

φ area fraction

Subscript:

av average

b bubble base

B bubble

calc calculated

d departure

exp experimental

F Fritz equation of bubble departure, equation (9)

ℓ liquid

m merging bubbles or multibubbles

s single bubble

sub subcooling

t total

v vapor

Literature Survey

As mentioned in the INTRODUCTION, bubble interference has been reported previously. The earliest mention of it was probably that found in reference 9. More recent experimental findings have been reported since then. In general, the bubble interference can be classified into two types, those of vertical interference and those of lateral interference. The vertical interference occurs between consecutive bubbles emitted from the same nucleation site in rapid succession. This type of bubble interference was called chain-bubbles interference in reference 9. It was also reported in references 6, 8, 10, and 11. This type of bubble coalescence was the model utilized in reference 8 to derive the criterion for the transition from the discrete-bubble regime to the merging-bubble regime. Deissler used a similar model for his analysis of burnout heat flux (ref. 12). The lateral type of bubble coalescence (or mushroom bubbles according to ref. 4) was the interference between the neighboring bubbles due to close proximity, a phenomenon not entirely unfamiliar to the urban or suburban dwellers. As observed in references 3, 4, and 13, a growing bubble, while still attached to the heating surface, would merge with a neighboring bubble. This merging could be caused either by contact of two growing bubbles or by the "up draught" of a departing bubble. The area of influence of each bubble has been found to be roughly 2 bubble radii away from the nucleation center (refs. 3 to 5). In either case, the lateral-merging bubbles could be pictured as mushrooms with two or more stems. These stems would be the places where vaporization occurs. This type of coalescence has been included in those boiling models postulated

in references 3 to 5. As will be shown later in the section RESULTS AND DISCUSSION, the mushroom bubbles are far more frequently observed than the chain bubbles. Therefore, the mushroom bubbles will be the ones discussed in this paper.

Since the lateral coalescence is due to the interference of neighbors, the distribution of bubbles should be known. In reference 14, it was found from the distribution of the sites on a boiling surface that the site population was distributed according to Poisson's equation

$$P_M(X) = \frac{e^{-M}(M)^X}{X!} \tag{1}$$

where $M = \overline{Na}/A$ and $X = Na/A$, but no attempt was made to predict the population distribution a priori; instead, the cell area, a, was used strictly as an empirical parameter to fit the data with Poisson curves.

Apparatus and Procedure

The test was carried on inside a 6-inch-diameter by 4-inch-high cylindrical tank made of stainless steel and provided with viewing windows. The tank had provisions for a fill, a drain, a pressure gage, electrical connections, thermocouple leads, and auxiliary heaters. The heater was a thin, electrically conductive, transparent coating 1/16-inch wide, 1-inch long deposited on a 1- by 1- by 1/8-inch heat-resisting glass plate. The plate was mounted horizontally on a small Bakelite bench with a mirror situated beneath the plate and inclined 45°. Thus, the camera aiming from a front window saw simultaneously a front view and a bottom view (through the mirror) of the image of any bubble generated on the heating surface. The plate was clamped down by two copper clamps which

also served as electrical leads. The actual heating area was 1/16 by 3/4 inch, since the two end areas were covered by the copper clamps (fig. 1). The 1/16-inch-wide strip was used instead of a wider heating area to assure that no more than two rows of bubbles were generated. This arrangement was necessary to avoid confusion in the front view because of the presence of overlapping rows of bubbles. Originally, an alternating-current source was used, but due to the low heat capacity of the heating film, there were 120-cycle-per-second temperature fluctuations on the heating surface. At lower heat flux, when bubble frequencies were low, this 120-cycle-per-second fluctuation apparently did not have a serious effect. However, as the heat flux was increased and bubble frequency fell in the vicinity of 120 cycles per second, the alternating-current fluctuation began to dictate the bubble frequency, and the bubbles began to grow in unison. Thus, only those runs where there was no apparent synchronization between bubbles and current waves were retained. Later, a direct-current source was used. However, because of the high voltage applied to the electrodes (60 to 120 v), electrolysis would take place if water was used. Thus, only methanol was used for direct-current runs. At the beginning of a series of runs, the tank was loaded with a fresh batch of pure methanol or distilled water. The liquid was preheated to a desired temperature by the auxiliary heater. The bulk temperature was constantly monitored through thermocouple readings, and the temperature level was controlled by turning the auxiliary heaters on and off. The auxiliary heaters were always off while actual test runs were being carried out. The test heater would be turned on, set at a desired heat flux by varying

the applied voltage, and then high-speed motion pictures (up to 5000 frames/sec) were taken. The simultaneous viewing of bubble activities from front and bottom (mirror image) was deemed necessary to get the true picture of bubble interaction. However, because of the difference in optical distance of the two views, it was extremely difficult to keep both views in sharp focus. Thus, the optical qualities of pictures were somewhat sacrificed. Because of such difficulties, studies were limited to those runs with a moderate amount of merging to maintain the accuracy of reading. The high-speed motion pictures were analyzed on a motion-picture analyzer. A total of 14 rolls were examined. For each roll, 50 to 100 frames were studied. The sample frames were selected by arbitrarily stopping the film 50 to 100 times at irregular intervals.

On each frame, information about each of the bubbles present on the entire heat surface 3/4 by 1/16 inch were measured and recorded. The raw data include:

(1) The location and size of each bubble (the size or diameter of a bubble is defined as the width of a bubble at its widest part. In a few instances, a mushroom bubble could have a very wide hovering bubble overcasting a large area. In such cases, the bubble size is defined as the width of the bubble stem below the height of an average single bubble. See fig. 2.)

(2) The classification of bubbles, namely, whether the bubble was a single bubble, or was merging with other bubbles. The criterion for the merging bubbles was the physical contact of two or more bubbles, while at least one bubble was still attached to the heating surface.

(3) The number of active bubbles involved in a merging bubble, and

(4) The total number of active bubbles n on that frame.

From the aforementioned raw data, calculations were made, and the following was deduced:

(1) The average size of single bubbles was made over all the single bubbles recorded in those sample frames. This was expressed in terms of the area fraction of influence of single bubbles, against the total area or φ_s. The area of influence of the bubble φ_s was computed by the equations

$$\varphi_s = \frac{\pi D_s^2}{A_t} \qquad \text{if} \quad D_s < W \tag{2a}$$

and

$$\varphi_s = \frac{2\,W\sqrt{D_s^2 - W^2} + D_s^2 \sin^{-1}\frac{W}{D_s}}{A_t} \qquad \text{if} \quad D_s > W \tag{2b}$$

The shaded areas in figure 3 are the areas of influence of single bubbles. Note that equation (2b) represents the area of a part of a circle with two segments cut off. The mean area fraction averaged over all the bubbles is

$$\varphi_{s,av} = \frac{\sum_{i=1}^{h} \varphi_{s,i}}{h} \tag{2c}$$

where h is the total number of all the single bubbles studied in the roll.

(2) The average size of the area covered by a merging bubble in a frame was expressed as the area fraction φ_m, which was calculated by summing up all the area fractions covered by each merging bubble in the

same frame. The area fraction of each merging bubble was also computed from equations (2a) and (2b), except that $D_m/2$ was used instead of D_s. The average area fraction of merging bubbles was computed over all the frames, or

$$\varphi_{m,av} = \frac{\sum_{i=1}^{k} \varphi_{m,i}}{k}$$

where k is number of sample frames and $\varphi_{m,i}$ is the sum of all the area fractions of merging bubbles in the frame i. Also computed for each roll of film was the standard deviation s associated with the $\varphi_{m,av}$

$$s = \sqrt{\frac{\sum_{i=1}^{k} (\varphi_{m,av} - \varphi_{m,i})^2}{k}}$$

(3) The average instantaneous bubble population density n_{av} was taken for the total number of sample frames, k.

The total number of active sites N seen in a given roll of film were also studied. The movie was projected on a paper and all the sites where bubbles had ever been generated were marked down. The range of conditions and the data are tabulated in table I.

RESULTS AND DISCUSSION

General Description of Photographical Observation

Before the quantitative study on bubble interferences, the following qualitative descriptions should be given:

(1) The merging of bubbles was predominately due to lateral coalescence. The merging took place when one growing bubble got into the area

of influence of a neighboring bubble. A detailed listing of bubble classification and raw data is contained in reference 15.

(2) The number of merging bubbles and the area covered by these merging bubbles increased with both the increase of bubble size and the instantaneous bubble population. With pressure and degrees of subcooling held constant, both the bubble size and the instantaneous bubble population increased with heat flux. Thus increasing the heat flux means increasing the area of merging bubbles.

(3) The location of merging bubbles appeared to be random. For a given location, at one moment there could be anything ranging from no bubbles, one bubble, several discrete bubbles, to merging bubbles. However, the probability of having merging bubbles increased with increasing heat flux.

Analysis

Based upon the general qualitative description of bubble interference observed photographically, a model will be postulated to account quantitatively for the area fraction covered by the merging bubbles. The analysis will be carried out in two steps: The first step will be to seek the relation between the area of a merging bubble with the quantities such as the mean area of influence of a bubble and the instantaneous bubble population, provided the latter two are given. The second step will be to attempt to estimate the area of influence and the instantaneous bubble population from the more basic information such as heat flux, subcooling, and total bubble population (or site population). The purpose is to estimate the area of merging bubbles from the aforementioned basic information.

(1) Basic Model - The basic model for bubble interference is described in the following manner:

(a) Each bubble has an area of influence, which is the area within 1-bubble-diameter distance from the nucleation center. This assumption is based upon the observations made in reference 3.

(b) Since each bubble grows, the area of influence is based upon the time-mean bubble size.

(c) Two bubbles will merge if one is located within the area of influence of the other.

(d) The bubbles are assumed to be distributed according to a Poisson distribution. This distribution is assumed to apply not only to site population as found in reference 14, but also to the instantaneous bubble population. Note that at any moment, only part of the sites are actively occupied by bubbles, while the rest are in the waiting period.

(2) Poisson Distribution - The following equation is used to express the previously postulated model in mathematical form:

$$P_\mu(x) = \frac{e^{-\mu}\mu^x}{x!} \tag{3}$$

where $P_\mu(x)$ is the percentage of cells each of which has x bubbles in it. while the average number of bubbles per cell is

$$\mu = \frac{n_{av}}{\frac{A_t}{A_s}} = \frac{n_{av}}{A_t} A_s = n_{av}\varphi_s \tag{4}$$

where A_s is the mean area of influence of a single bubble or the area of a cell, n_{av} is the average instantaneous bubble population on a total

heating area A_t, and φ_s is the area fraction A_s/A_t. Note that equations (1) and (3) are similar in form except that the site population N was used in equation (1), while the instantaneous bubble population n was used in equation (3) and that in equation (3) the cell area was defined as the area of influence of a bubble.

Since it is assumed that bubbles will merge when two or more bubbles are present in one cell, the percentage of cells that contain merging bubbles is

$$P_\mu(x > 2) = \sum_{x=2}^{\infty} P_\mu(x) \tag{5a}$$

or

$$P_\mu(x > 2) = 1 - P_\mu(0) - P_\mu(1) = 1 - e^{-n_{av}\varphi_s}(1 + n_{av}\varphi_s) \tag{5b}$$

Since $P_\mu(x > 2)$ is by definition the percentage of cells covered by two or more bubbles or merging bubbles, it is the area fraction covered by merging bubbles

$$\varphi_m = P_\mu(x > 2) = 1 - e^{-n_{av}\varphi_s}(1 + n_{av}\varphi_s) \tag{6}$$

This equation will give the area fraction of merging bubbles if the mean instantaneous bubble population n_{av} and mean area of influence of a single bubble are known. These two terms can either be obtained experimentally or analytically. The next two sections constitute the second step of analysis, namely, determination of n_{av} and A_s analytically.

(3) Mean Area of Influence of a Single Bubble - According to the assumed basic model, the mean area of influence is the area within 1 bubble diameter from the nucleation center, and the bubble diameter is the time average of a growing bubble

$$D_{av} = \frac{1}{t_g}\int_0^{t_g} D(t)dt \qquad (7)$$

or

$$R_{av} = \frac{1}{t_g}\int_0^{t_g} R(t)dt \qquad (7a)$$

The term bubble radius $R(t)$ can be obtained through bubble growth information. Although many theoretical equations are available, it is more convenient to use the empirical expression $R = at^b$, where $b = 0.4$ (ref. 16) will be used. Since the process of computing the time-average radius R_{av} involves integration of $R(t)$, small deviations in $R(t)$ usually will be evened out. Thus

$$R_{av} = \frac{a}{t_g}\int_0^{t_g} t^b dt = \frac{at_g^b}{b+1} = \frac{R_d}{1+b} = \frac{R_d}{1.4} \qquad \text{if } b = 0.4 \qquad (7b)$$

As to the departure radius R_d, Staniszewski's empirical expression will be used

$$R_d = R_F(1 + 10.44\,\dot{R}_d) \qquad (8)$$

where R_F is the departure radius according to Fritz' equation

$$R_F = 0.4215\,\beta\sqrt{\frac{2\sigma}{g(\rho_l - \rho_v)}} \qquad (9)$$

$\dot{R}_d$ is in feet per second, β is the contact angle in radians, and R is in feet.

Unfortunately the growth rate at departure $\dot{R}_d$ involved in the above equation can no longer be calculated from the expression $R = at^b$, partly because the exponent b actually varies with time and partly because the coefficient a should be a function of an experimental condition such as

heat flux, subcooling, pressure, cavity size, etc. Thus an expression for the growth rate $\dot{R}$ as a function of the test condition should be used.

Although many bubble growth equations are available, only a few considered the effect of the bulk turbulence by including terms that describe the thermal layer or the heat dissipation to the bulk. Among such equations are those proposed in references 3, 17, and 18. The equation in reference 17 would be quite convenient to use if both ΔT_w and q_w were known. Unfortunately, the growth expressions in references 3 and 18 are rather clumsy to use. However, if only the bubble growth rate at departure is of interest, the situation is somewhat simpler because of the fact that in the later stage of bubble growth the sensible heat stored in the superheated layer enveloping the bubble should have been long since exhausted. Therefore the bubble should be receiving heat only from the bubble base. (This heat may be in the form of evaporation of microlayer as shown in ref. 19.) While losing heat to the surrounding bulk, the bubble growth rate at departure can be easily derived by following the procedure in reference 3

$$\dot{R} = \frac{1}{\lambda \rho_v} \left(\frac{A_b}{A_B} q - \frac{K \Delta T_{sub}}{\delta} \right) \tag{10}$$

where $\frac{A_b}{A_B} \simeq 0.25$ if the bubble at departure can be assumed as a truncated sphere with contact angle between 45° to 60° (c.f., ref. 3) and the δ is the thermal layer thickness. The information about thermal layer thickness of a boiling fluid is very meager, but there are a few measurements (ref. 6

and 20). Therefore, if the thermal layer thickness δ is known, by using equations (8) to (10), the bubble departure size can be determined.

(4) Instantaneous Bubble Population - The instantaneous bubble population should be differentiated from the commonly used term "bubble population". The latter actually is a misnomer. When the number of bubble columns are counted during the running of a motion picture or the number of aureole left on a plate after boiling, only the population of the bubble nucleation sites is shown, but not the bubble population at any moment. The relation between site population N and the instantaneous bubble population n can be likened to that between the number of houses in a block and the number of families actually at home at a given moment. It is easy to see that these two populations can be tied by the equation

$$n_{av} = \frac{t_{g,av}}{t_{g,av} + t_{w,av}} N = t_{g,av} f_{av} N \qquad (11)$$

The variation of N as function of q has been reported in many places, and, unfortunately, the result varies widely. The difficulty stems from the diversity of surface condition and hysteresis (refs. 2, 6, and 21). Unless some characteristic parameter other than rms roughness of a surface can be found to account for size distribution of cavity, it is futile to try to correlate N against q. However, the site population N is still a quantity much easier to determine experimentally than the instantaneous bubble population n. Thus, it is still worthwhile to obtain n through N.

The mean frequency f_{av} can easily be determined through the expression in reference 17

$$fD = 0.59 \frac{(\rho_l - \rho_v)g\sigma}{\rho_l^2} \tag{12}$$

so

$$f_{av} = \frac{0.59}{D_{d,av}} \left[\frac{(\rho_l - \rho_v)g\sigma}{\rho_l} \right]^{1/4} \tag{13}$$

The time of growth period t_g can readily be calculated through

$$R_d = \int_0^{t_g} \dot{R}\, dt \tag{14}$$

provided $\dot{R}(t)$ and R_d are known. As mentioned before, if an empirical expression is used

$$R_d = at_g^b \tag{15}$$

$$\dot{R}_d = abt_g^{b-1} \tag{16}$$

$$\frac{R_d}{\dot{R}_d} = \frac{t_g}{b}$$

or

$$t_g = \frac{bR_d}{\dot{R}_d} \tag{17}$$

Thus from equations (8), (10), and (17) the growth period t_g can be calculated. Strictly speaking, equation (10) can be used to replace equation (16), only when the empirical form (eq. (16)) is identical to the analytical form (eq. (10)). However, an underestimated growth rate $\dot{R}$ tends to give an overestimated growth period t_g and an underestimated departure diameter D_d. The result is that the two errors tend to compensate each other in the product of mean bubble population and mean area of influence

$$n_{av}A_s = t_g \frac{(fD)_d}{D_d} \pi D_d^2 \qquad (18)$$

(5) Calculation of Area Fraction Covered by Influence of a Single Bubble $(\varphi_{s,av})_{calc}$ from $(D_{av})_{calc}$ - The mean influence area fraction covered by a single bubble can be computed from the time-averaged diameter of a bubble D_{av} by using equations (2a) and (2b), except that D_{av} will be used in the place of D. The φ_s thus computed will be $(\varphi_{s,av})_{calc}$. Strictly speaking, $(\varphi_{s,av})_{calc}$ should be an average of $(\varphi_s)_{calc}$ which, in turn, should be computed from D(t) as shown in equation (2c). Since only an estimation was intended, $(\varphi_{s,av})_{calc}$ can be directly computed from $(D_{av})_{calc}$.

Comparison of Experimental Data with Analysis

The quantitative result will be compared with the model derived in the section Analysis in two steps also. The first step will be to check whether the area fraction of merging bubbles φ_m based upon the Poisson distribution (eq. (6)) can be used to relate φ_m with the experimental values of the mean area of influence of a single bubble $\varphi_{s,exp}$ and the mean instantaneous bubble population $n_{av,exp}$. The second step will be to test whether equations (8) and (11) can be used to predict $\varphi_{s,exp}$ and $n_{av,exp}$ respectively and whether the calculated product $(\varphi_s n_{av})_{calc}$ can be used to predict the merging bubble area fraction $\varphi_{m,exp}$.

(1) The Relation Between Area Fraction of Merging Bubbles φ_m Against Product of Measured Values of Mean Area of Influence of Single Bubbles and Mean Instantaneous Bubble Population $(n_{av}\varphi_s)_{exp}$ (i.e., the average number of bubbles per cell) - To test equation (6), $(\varphi_{m,av})_{exp}$

was plotted against $(n_{av}\varphi_{s,av})_{exp}$ in figure 4(a). The solid curve represents equation (6). Each circle represents the mean values obtained from one roll of film. Figure 4(b) shows a similar plot on rectangular coordinates to show the standard deviations associated with each area fraction of merging bubbles for the samples studied. Judging from the figures, the model is fairly close. Thus, if the mean bubble population n_{av} and the mean area of influence of single bubbles φ_s are given, the area covered by merging bubbles can be calculated. The values of n_{av} and $\varphi_{s,av}$ can either be obtained experimentally in the same way that figure 4 was constructed, or they can be estimated from test conditions through bubble departure size, bubble growth rate, and frequency by using the available equations.

(2) Comparison of Calculated and Measured Bubble Departure Diameters $D_{d,cal}$ Against $D_{e,exp}$ - To estimate $\varphi_{s,av}$, it is necessary to know the departure diameter D_d. Equations (8) and (9) were used to compute D_d with departure growth rate $\dot{R}_d$ computed from equation (10). The thermal layer thickness δ used in equation (10) was determined from the experimental measurement in reference 10 by matching the heat-transfer coefficient for the case of water (varying roughly around 2×10^{-3} ft). For the case of methanol, the thermal layer thickness was assumed to be 2×10^{-3} feet. The calculated values of D_d are then compared with the experimental ones derived through equation (7). The comparison is shown in figure 5. It can be seen that most points are within a ±20 percent error limit, which is about the same as the 25 percent error limit of equation (8).

(3) Comparison of Calculated and Measured Mean Instantaneous Bubble Population $n_{av,calc}$ Against $n_{av,exp}$ - To test equation (11), the mean instantaneous bubble population n_{av} was calculated from the experimentally determined site population N together with the calculated frequency f_{av} and growth period $t_{g,av}$. The bubble frequency f_{av} was calculated from equation (13) by using the calculated departure diameter $D_{d,cal}$. The growth period $t_{g,av}$ was calculated from equation (17) by using $D_{d,calc}$ and $\dot{R}_{d,calc}$ (from eq. (10)). The comparison with $n_{av,exp}$ is shown in figure 6. The ±60 percent error limits are also shown in the figure, which are the error limits associated with equation (12).

(4) Comparison of Measured Merging Bubble Area Fraction $(\varphi_m)_{exp}$ with That Obtained From the Calculated Average Instantaneous Bubbles Per Cell $(n_{av}\varphi_s)_{calc}$ - By using equations (2a) and (2b), $\varphi_{s,av}$ was computed from $D_{av,calc}$. In figure 7, the product $(\varphi_{s,av}n_{av})_{calc}$ was plotted with the average area fraction of merging bubbles $\varphi_{m,av}$. Also shown in figure 7 is the theoretical curve from equation (6). Although there is scattering, the result is still quite gratifying considering all the crude assumptions being made and the large error limits associated with empiricism of equations (8) and (12). Thus, it is shown that an estimate of the area covered by merging bubbles can be based upon the test conditions (heat flux, pressure, subcooling, etc.) provided that the site population is known.

CONCLUDING REMARKS

In the nucleate-boiling regime, if both discrete bubbles and merging bubbles are present, the overall heat-transfer coefficient will have to be determined by considering the contribution due to both bubbling mechanisms. Even if the heat-transfer process of each mechanism was known, a weighting factor is needed to determine the relative contribution of each mechanism.

One possible weighting factor would be the area fractions of merging bubble and discrete bubbles. Based upon the result obtained from the boiling of methanol and water on a narrow heating strip, it is found that the transition from the discrete-bubble regime to the merging-bubble regime is gradual. Furthermore, the results showed that area fraction of merging bubble can be predicted satisfactorily from the Poisson distribution if the average number of bubbles per cell (the cell is defined as the average area of influence of a single bubble) is known.

It is desirable to be able to determine the average number of bubbles per cell a priori. A method of estimating this item based upon crude assumptions and empirical equations was proposed in this report. The maximum error associated with the estimated values was roughly 100 percent, which might be due to the large errors introduced in the basic empirical equations. If a better method is available for estimating the bubble size and bubble population, more accurate estimations of the number of bubbles per cell and, thus, of the area fraction of merging bubbles might be possible.

REFERENCES

1. Westwater, J. W.: Boiling Heat Transfer. Advances in Chem. Eng., Vol. 1, T. B. Drew and J. W. Hoops, eds., Academic Press, 1956.

2. Jakob, Max: Heat Transfer. Second ed., ch. 29, John Wiley & Sons, Inc., 1950.

3. Hsu, Yih-Yun, and Graham, Robert W.: An Analytical and Experimental Study of the Thermal Boundary Layer and Ebullition Cycle in Nucleate Boiling. NASA TN D-594, 1961.

4. Gaertner, R. F.: Photographic Study of Nucleate Pool Boiling on a Horizontal Surface. Paper 63-WA-76, ASME, 1963.

5. Zuber, Novak: Nucleate Boiling. The Region of Isolated Bubbles and the Similarity with Natural Convection. Int. Jour. Heat and Mass Transfer, vol. 6, no. 1, Jan. 1963, pp. 53-78.

6. Yamagata, Kiyoshi, Hirano, Fujio, Nishikawa, Kaneyasu, and Matsuoka, Hisamitsu: Nucleate Boiling of Water on the Horizontal Heating Surface. Kyushu Imperial Univ. Faculty of Eng. Memoirs, vol. 15, no. 1, 1955, pp. 97-163.

7. Kirby, D. B., and Westwater, J. W.: Photography from Below: Nucleate Boiling on Electrically-Heated Horizontal Glass Plates. Chem. Eng. Sci., vol. 18, no. 7, July 1963, p. 469.

8. Moisses, Raphael, and Berenson, Paul J.: On the Hydrodynamic Transitions in Nucleate Boiling. Paper 62-HT-8, ASME, 1962.

9. van Krevelen, D. W., and Hoftijzer, P. J.: Studies of Gas-Bubble Formation - Calculation of Interfacial Area in Bubble Contactors. Chem. Eng. Prog., vol. 46, no. 1, Jan. 1960, pp. 29-33.

10. Nishikawa, Kaneyasu: Nucleate Boiling Heat Transfer of Water on the Horizontal Roughened Surface. Kyushu Imperial Univ. Faculty of Eng. Memoirs, vol. 17, no. 2, Jan. 1958, pp. 85-103.

11. Stock, Bernard J.: Observations on Transition Boiling Heat Transfer Phenomena. ANL-6175, Argonne Nat. Lab., June 1960.

12. Cole, Robert: A Photographic Study of Pool Boiling in the Region of Critical Heat Flux. Preprint 21, A.I.Ch.E., 1960.

13. Semeria, R. L.: An Experimental Study of the Characteristics of Vapour Bubbles. Paper 7, Symposium on Two-Phase Fluid Flow, Inst. Mech. Eng. (London), Feb. 7, 1962.

14. Gaertner, R. F.: Distribution of Active Sites in the Nucleate Boiling of Liquids. A.I.Ch.E. Chem. Eng. Prog. Symposium Ser., vol. 59, no. 41, 1963, p. 52.

15. Hsu, Yih Yun: Gradual Transition of Nucleate Boiling From Discrete Bubble Regime to Multibubble Regime. NASA TN (to be published).

16. Strenge, P. H., Orell, Aluf, and Westwater, J. W.: Microscopic Study of Bubble Growth During Nucleate Boiling. A.I.Ch.E. Jour., vol. 7, no. 4, Dec. 1961, pp. 578-583.

17. Zuber, Novak: Hydrodynamic Aspects of Nucleate Pool Boiling. Pt. I - The Region of Isolated Bubbles. RW-RL-164, Ramo-Wooldridge, Jan. 27, 1960.

18. Han, Chi-Yeh, and Griffith, Peter: The Mechanism of Heat Transfer in Nucleate Pool Boiling. Rep. 19, Dept. Mech. Eng., M.I.T., Mar. 30, 1962.

19. Hendricks, Robert C., and Sharp, Robert R.: Initiation of Cooling Due to Bubble Growth on a Heating Surface. NASA TN (to be published).

20. Treschev, G. G.: Experimental Investigation of the Mechanism of Heat Transfer in Surface Boiling. Teploenergetika, vol. 4, no. 5, 1957, pp. 44-48.

21. Graham, Robert W., and Hendricks, Robert C.: A Study of the Effect of Multi-g Accelerations on Nucleate-Boiling Ebullition. NASA TN D-1196, 1963.

TABLE I. - COMPILATION OF DATA

Run number	Test fluid	Bulk temperature, ^{o}F	Heat flux, q, $\frac{Btu}{(hr)(sq\ ft)}$	ΔT_{sub}, ^{o}F	Total number of frames studied, k	Total number of single bubbles studied in roll, h	Number of merging bubbles studied	Average instantaneous bubble population, n_{av}	Average area fraction of influence of bubble, $\varphi_{s,av}$	Average area fraction of merging bubbles, $\varphi_{m,av}$	Standard deviation associated with $\varphi_{m,av}$	Total number of bubble sites, N
62-12-4-1	H_2O	201	21,150	11	101	128	87	2.13	0.121	0.0451	0.0451	13
62-12-4-2		197	23,950	15	100	162	43	2.05	.102	.0182	.0451	10
62-12-4-3		198	32,000	14	102	172	51	2.19	.109	.0240	.0649	15
62-12-4-5		199	49,500	13	99	268	57	3.28	.138	.0402	.0936	18
62-12-4-6		196	41,500	16	102	193	35	2.24	.128	.0171	.0533	19
63-1-14-6	CH_2OH	132	48,300	16	96	328	57	4.01	0.127	0.0385	0.0714	18
63-2-6-1		137	92,900	11	50	139	86	4.50	.169	.115	.135	21
63-2-6-2		137	104,900	11	56	155	187	6.11	.168	.255	.225	20
63-2-6-3		140	120,700	8	47	130	202	7.06	.184	.3695	.214	30
63-2-6-4		139	135,000	9	50	92	373	9.30	.167	.535	.216	30
63-7-2-2		128	73,100	20	55	135	447	10.58	.159	.470	.183	19
63-7-8-1		111	68,400	37	70	263	196	6.56	.103	.110	.117	20
63-7-8-4		119	88,200	29	56	119	472	10.55	.112	.358	.167	26
63-7-8-5		119	82,600	29	49	124	385	10.39	.115	.327	.152	27

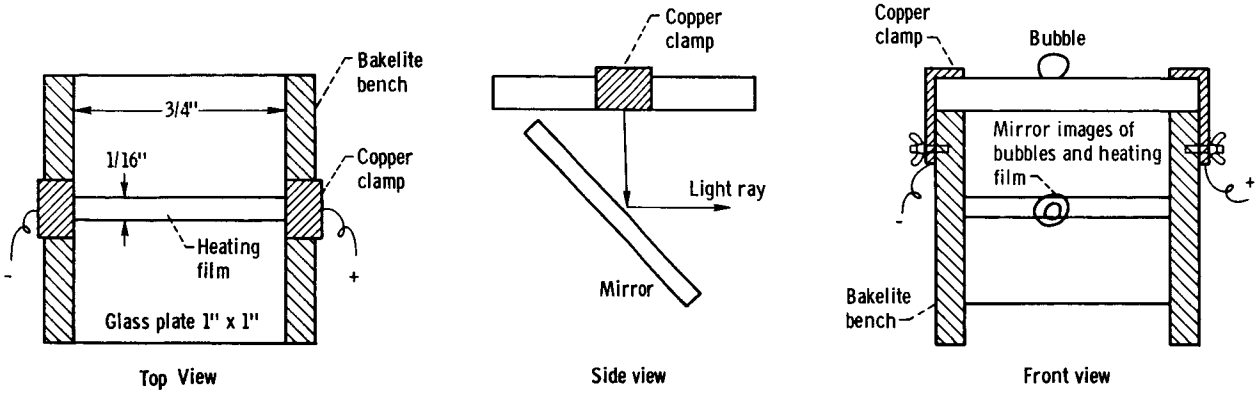

Figure 1. - Setup of heating element.

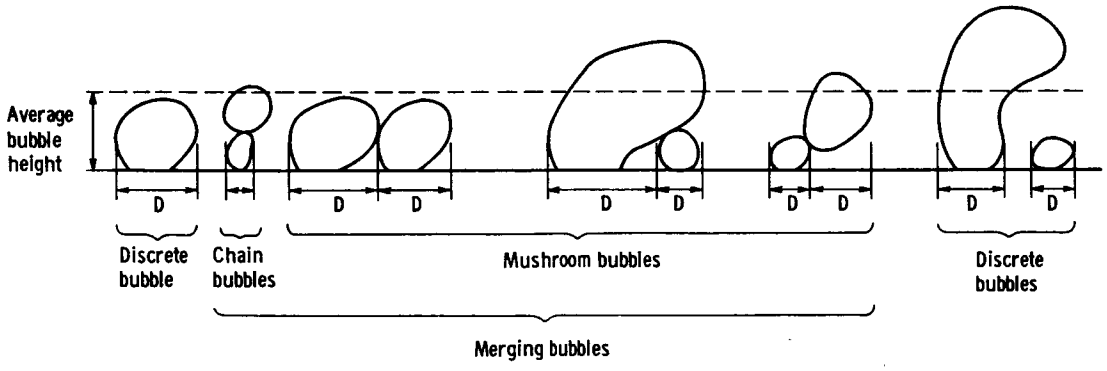

Figure 2. - Various configurations of bubbles.

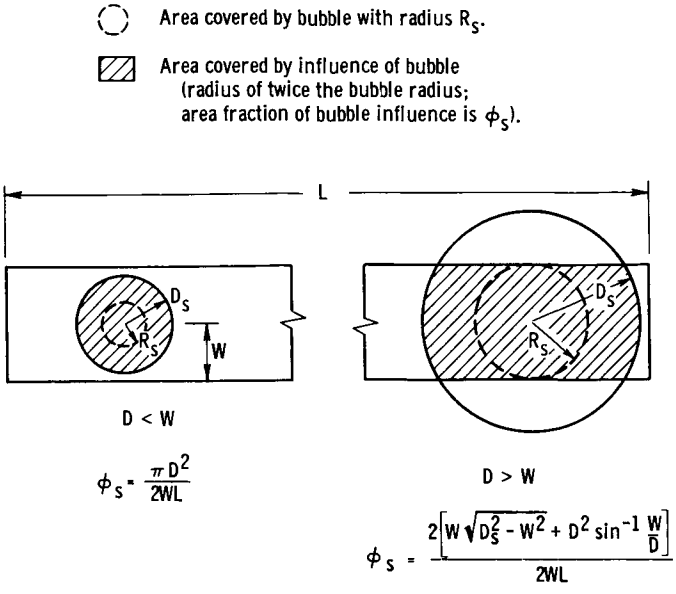

Figure 3. - Calculation of area fraction of heating strip covered by influence of bubble.

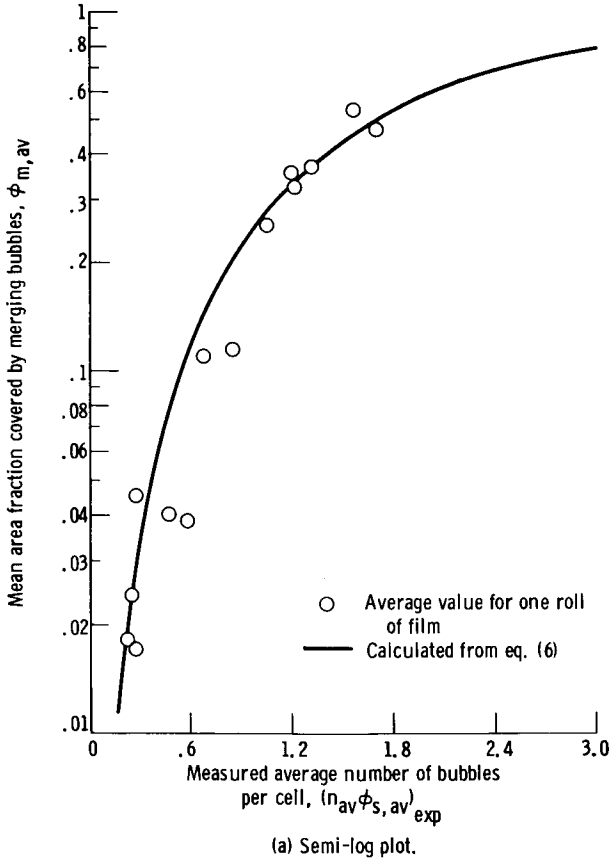

(a) Semi-log plot.

Figure 4. - Area fraction of merging bubble as a function of measured average number of bubbles per cell.

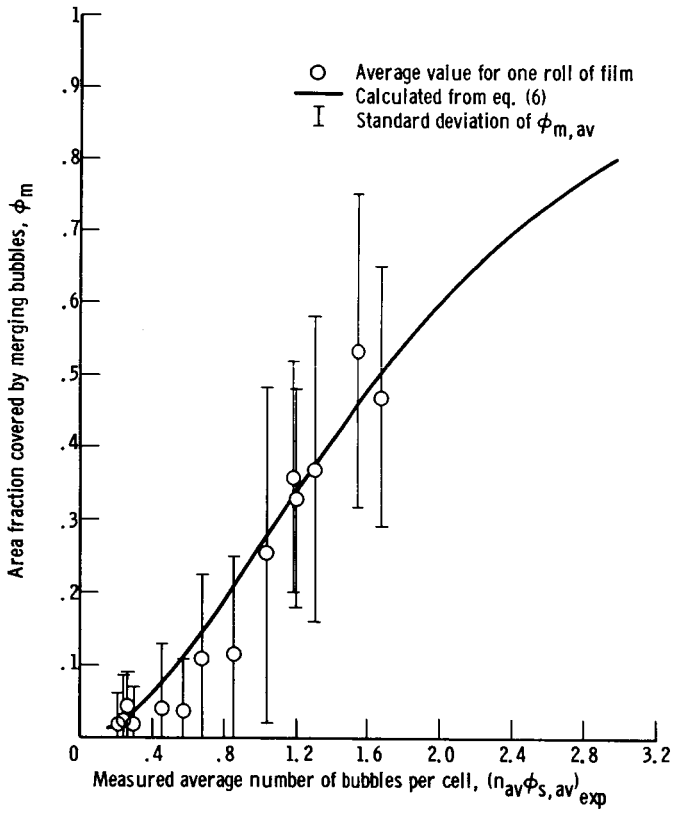

(b) Rectangular plot showing standard deviation.

Figure 4. - Concluded. Area fraction of merging bubble as a function of measured average number of bubbles per cell.

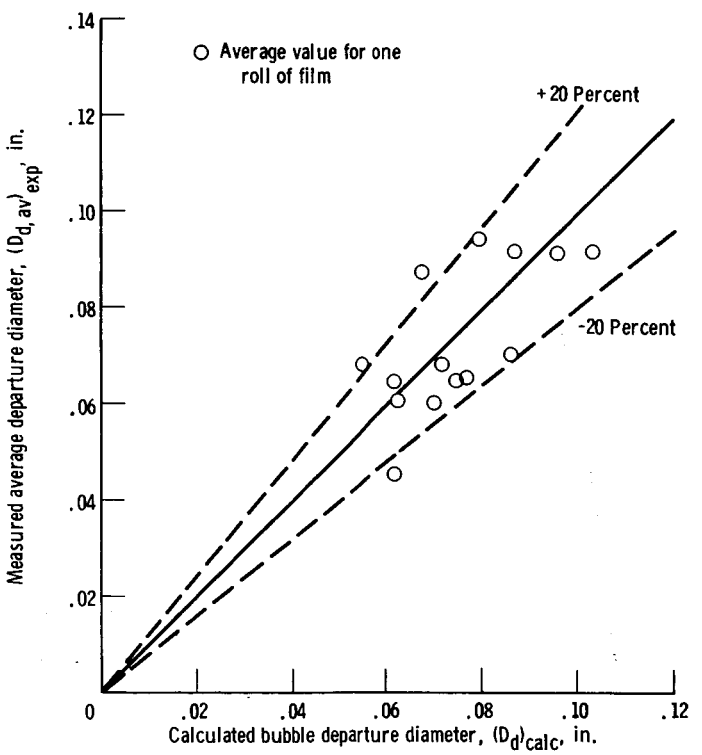

Figure 5. - Comparison of calculated and measured bubble departure diameters.

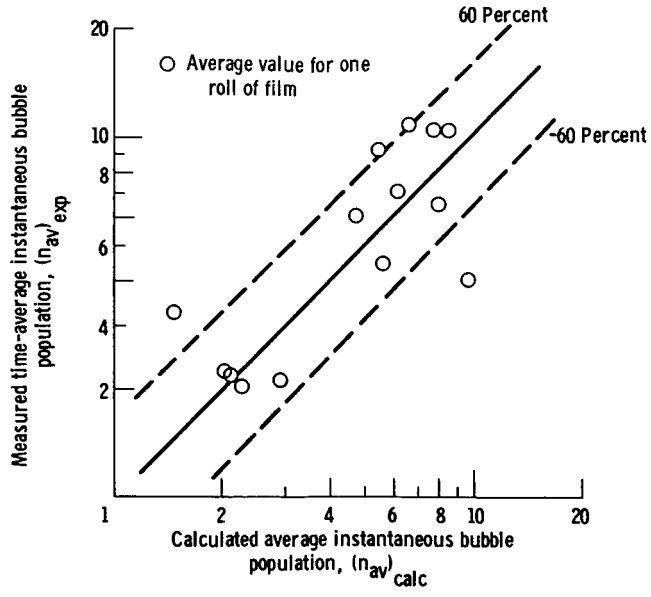

Figure 6. - Comparison of calculated and experimental values of average instantaneous bubble population.

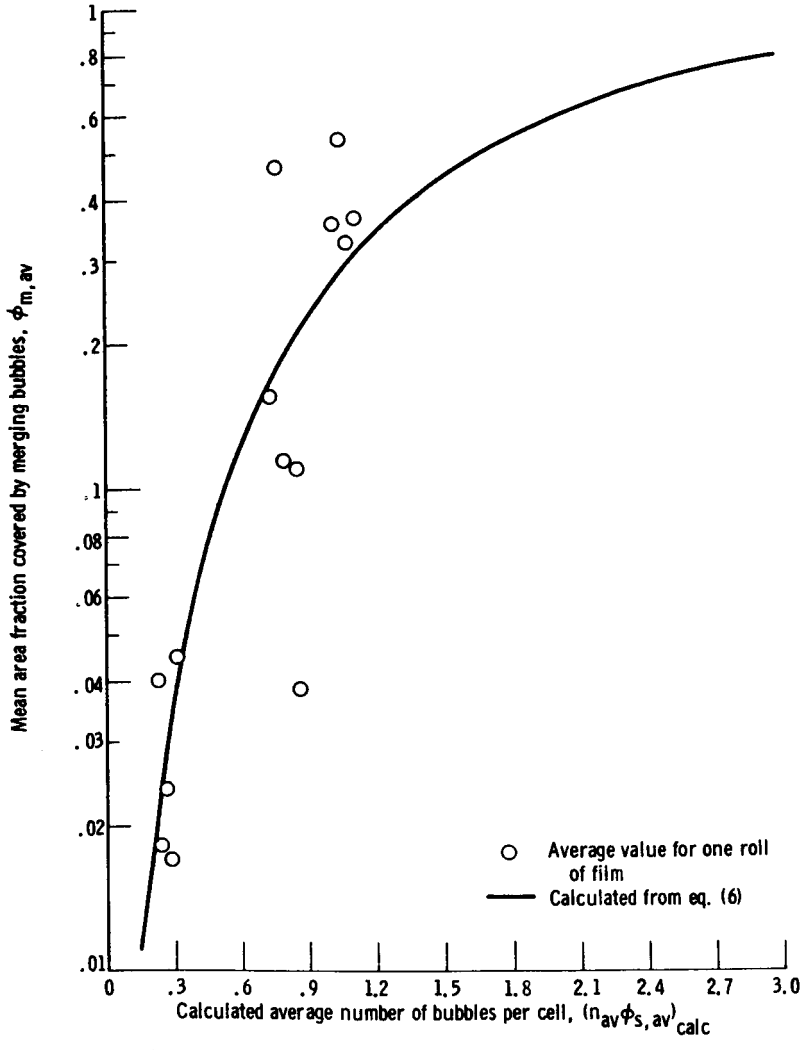

Figure 7. - Area fraction of merging bubbles as a function of calculated average number of bubbles per cell.